Stationary and traveling solitons via local dissipation in Bose-Einstein condensates in ring optical lattices

Russell Campbell* and Gian-Luca Oppo
SUPA and Department of Physics, University of Strathclyde, 107 Rottenrow, Glasgow G4 0NG, United Kingdom
(Received 22 June 2016; published 13 October 2016)

A model of a Bose-Einstein condensate in a ring optical lattice with atomic dissipations applied at a stationary or at a moving location on the ring is presented. The localized dissipation is shown to generate and stabilize both stationary and traveling lattice solitons. Among many localized solutions, we have generated spatially stationary quasiperiodic lattice solitons and a family of traveling lattice solitons with two intensity peaks per potential well with no counterpart in the discrete case. Collisions between traveling and stationary lattice solitons as well as between two traveling lattice solitons display a critical dependence from the lattice depth. Stable counterpropagating solitons in ring lattices can find applications in gyroscope interferometers with ultracold gases.

DOI: 10.1103/PhysRevA.94.043626

I. INTRODUCTION

Bose-Einstein condensates (BECs) trapped in an optical lattice have attracted major scientific interest and can provide an interesting analog to solid-state systems [1,2]. An advantage here is that there is almost complete control of the parameters that regulate the lattice. This has led to studies of solid-state phenomena such as quantum phase transitions [3], transport [4], Anderson localization [5], and the macroscopic Zeno effect [6]. In the superfluid phase of the BEC, a lot of attention has been devoted to discrete breathers in the discrete nonlinear Schrödinger equation (DNLSE) [7] and to lattice solitons in the Gross-Pitaevskii equation (GPE) [8]. The optical lattice allows solitons and discrete breathers to exist with repulsive BEC where they have been observed experimentally [9]. Methods for the generation of discrete breathers include the evolution from Gaussian wave packets [10,11] and the relaxation from random-phase states via localized losses [12]. Stabilization of discrete breathers in the DNLSE via localized losses can be achieved by either the progressive lowering of the fluctuating background [7,12] or by producing sudden atomic avalanches [13]. Moving discrete breathers have also been obtained with these techniques in accurate numerical simulations. An interesting application of moving breathers is in atom interferometry [14]. Without a lattice, methods of soliton interferometry have been implemented experimentally in [15], while techniques for generating counterpropagating solitons by using a splitting potential barrier in a ring trap have been proposed and discussed in [16–18]. The aim of our work is to demonstrate that stationary and moving lattice solitons in continuous models of BECs in ring lattices can be generated and stabilized via localized losses. In particular we show that higher-order lattice solitons that have no counterpart in the discrete case can be effectively stabilized by these techniques. Bright and dark lattice solitons were generated via dissipation for attractive BECs in [19]. Here we focus instead on repulsive BECs.

We consider a ring trap [20] with a toroidal optical lattice as realized, for example, in [21–24] [see Fig. 1(a)]. Experimentally, a BEC in a ring trap with an azimuthal optical lattice can be achieved either by using counterpropagating laser beams in a circular wave guide or by illuminating transversally a ring trap with two counterrotating orbital angular momentum laser beams with the optical axis along the center of the ring trap and perpendicular to the trap.

It is important to outline that the equations used in this paper for the case of a BEC in an optical lattice also describe light traveling through arrays of optical waveguides. Since the theoretical and experimental pioneering work of [25], lattice solitons, also known as gap solitons, have been predicted and observed in a variety of purely optical configurations [26]. In nonlinear optics, the ring lattice described above for a BEC corresponds to a cylindrical array of optical waveguides [see Fig. 1(b)]. All the results presented here can then be extended to this purely optical case. Lattice solitons in optical ring configurations have been investigated in [27], where the effects of self-interacting soliton tails have been studied in detail. Here we consider a number of optical waveguides that is large enough to make these effects negligible.

Another method of supporting solitons in nonlinear media is that of localized gain (for a review, see [28]). There is also great interest in parity-time symmetric systems [29], for which, when applied to a BEC, localized gain and dissipations are balanced (for recent reviews about nonlinear systems, see [30]). In our model, we believe that it would be possible to implement this technique too, with the gain being provided by an atom laser [31]. Indeed, such a setup is described in [32] for a ring trap without a lattice. In this paper, however, we focus on the effects of dissipation alone, where Hermitian or non-Hermitian Hamiltonians cannot be applied.

Since the GPE and the DNLSE have been obtained under the mean-field approximation, which is valid in the limit of large numbers of atoms, we do not consider here purely quantum effects arising from atom-atom correlation, such as the collapse and revival of the matter wave field [33] or many-particle entanglement [34,35]. A detailed investigation of these effects is beyond the scope of this paper, although recent studies concerning localization of a BEC in an optical lattice in the presence of localized dissipations and beyond the mean-field approximation can be found in [35–37]. All these simulations confirm that the fundamental result

*russell.campbell@strath.ac.uk

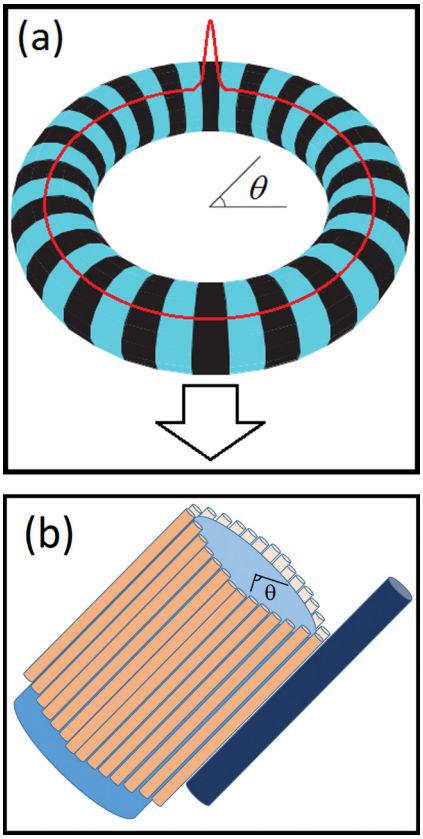

FIG. 1. (a) BEC lattice soliton in an optical lattice ring trap. The arrow identifies the position where localized losses are applied. (b) An array of optical waveguides in a ring configuration. The dark cylinder represents an output coupler capable of removing light from the array.

of self-localization via localized losses, originally obtained in [12], survives in the quantum regimes beyond the mean-field approximation.

Model equations for a BEC in a ring optical lattice are introduced in Sec. II. These are the continuous counterpart of the DNLSE with the addition of localized dissipations. In order to differentiate and compare the solutions of the continuous model of Sec. II with those of the DNLSE, we refer to continuous soliton solutions in the annular periodic potential as lattice instead of discrete solitons. Lattice solitons are also known as "gap solitons" in the literature. In Sec. III we discuss the generation of symmetric and asymmetric lattice solitons via the effect of stationary localized losses and compare them successfully to those found by other numerical methods in [38]. Traveling lattice solitons (TLSs) in the ring trap are generated and investigated in Sec. IV. Two kinds of TLSs are found: with one peak per lattice well and with two peaks per lattice well. It is important to note that the double-peak TLS has no counterpart in the DNLSE. Finally, collisions between traveling and stationary lattice solitons in a ring trap are investigated in Sec. V, while collisions between two traveling lattice solitons are studied in Sec. VI. In the DNLSE, collisions of discrete breathers were studied in [39], where their dependence on the velocity, amplitude, and phase difference of the breathers was investigated. Here we investigate the dependence of the collision of continuous lattice solitons on potential depth V_0. Possible applications to atom interferometry are discussed in the conclusions.

II. THE MODEL EQUATIONS

We consider the Gross-Pitaevskii equation for a one-dimensional BEC in an optical lattice given by [38,40]

$$i\hbar\frac{\partial\Psi(x,T)}{\partial T}=\left[-\frac{\hbar}{2m}\frac{\partial^2}{\partial x^2}+E_0\sin^2\left(\frac{\pi x}{L}\right)+g_{1D}|\Psi|^2\right]\Psi, \tag{1}$$

where $\hbar$ is the reduced Planck's constant, E_0 is the potential depth (usually measured with respect to the recoil energy), $L=\lambda/2$ is the lattice period, λ is the laser or spatial wavelength used for the optical lattice, and m is the atomic mass. The one-dimensional atom-atom interaction parameter is given by $g_{1D}=2\hbar\omega_\perp a_s$, where $\omega_\perp$ is the transverse trapping frequency and a_s is the scattering length of the BEC.

To describe the BEC trapped in the ring we use Eq. (1) with periodic boundary conditions. For convenience, dimensionless variables are used. First, we rewrite Eq. (1) by normalizing $u=\sqrt{L/2N}\Psi$, $t=T/T_0$, and $V_0=E_0/E_r$, where $T_0=mL^2/4\hbar$, $E_r=4\hbar^2/mL^2$ is the recoil energy, and N is the number of atoms [38]. The length scale x is then changed into the ring angle $\theta=2\pi x/ML$, ranging from 0 to 2π rad, where M is the number of potential wells in the ring along the azimuthal direction. The resulting equation is

$$i\frac{\partial u(\theta,t)}{\partial t}=\left[-\frac{\pi^2}{2M^2}\frac{\partial^2}{\partial\theta^2}+V_0 sin^2\left(\frac{M\theta}{2}\right)+\beta|u|^2-i\rho(\theta,t)\right]u. \tag{2}$$

The nonlinear parameter $\beta=N\omega_\perp a_s mL/\hbar$ is positive for repulsive condensates and negative for attractive ones. In order to describe localized losses of the atomic population along the ring at certain times t, we have added the term $-i\rho(\theta,t)u$ in Eq. (2). Extremely precise methods for removing atoms in a particular position of a BEC in optical lattices have been implemented with the use of narrow electron beams [41]. The intensity of such electron beams can control the number of atoms that are removed from one or more potential wells of the optical lattice. In our examples here, localized losses are applied at the furthest point in the ring (i.e., at an angular distance of π rad) from the peak of the stationary or moving lattice soliton. For example, with the stationary lattice solitons that are usually generated at $\theta=\pi$, the dissipation is applied at $\theta=0=2\pi$.

Equation (2) is normalized so that at $t=0$, before any atoms are lost due to dissipation,

$$\int u(t=0)\,d\theta=1. \tag{3}$$

In this paper, we use only repulsive BECs (i.e., $\beta>0$) and investigate the generation of bright lattice solitons via localized dissipations. We note that in [19] both bright and dark solitons have been generated via dissipation for attractive BECs and at moderate lattice depths. We have not observed generation of dark solitons in our simulations, but that does not exclude

them from being stabilized after a transient application of the dissipation.

III. STATIONARY LOCALIZED DISSIPATIONS

Stationary and moving breathers can be formed in the DNLSE starting from initial Gaussian wave packets [7,10,11]. For our continuous-variable model, we use the general form

$$u(t=0) = \frac{M^2}{\gamma^{1/2}\pi^{9/4}} \exp\left(-\frac{(\theta-\theta_c)^2}{2\gamma^2}\right), \tag{4}$$

with θ_c being the position of the center of the wave packet and γ being the width. With the nonlinear coefficient fixed at $\beta = 1$, the initial width was changed, and several localized solutions were found in the case of zero losses (i.e., the conservative case).

Typically, the Gaussian wave packet would reshape into a solitonic profile. The atomic mass expelled from the wave packet, however, forms a noisy background. The peak fluctuates in height as it keeps interacting with the background. As the width of the initial wave packet is increased, the background becomes noisier, and sometimes, smaller-amplitude peaks appear close to the main one. The small-amplitude peaks, however, do not survive in the long term. When the width of the initial Gaussian condition is too large, no peak is formed, and the condensate disperses into the background. Similarly, if the width is too small (smaller than a single potential well), there is no self-localization either.

When dissipation is applied to the above configuration, we obtain less noisy backgrounds since the mass expelled from the initial wave packet escapes at the location of the losses. In all the examples in this section, the dissipation acts on around four potential wells, with the maximum loss of 0.5 at $\theta = 0 = 2\pi$. For Gaussians of different widths we routinely recover stable lattice soliton solutions via localized dissipation (see, for example, Fig. 2). These solutions are very close to those shown in [38] and are obtained with very different numerical methods.

The effect of dissipation on the soliton and background can be seen clearly in Fig. 3, which shows the decay of the

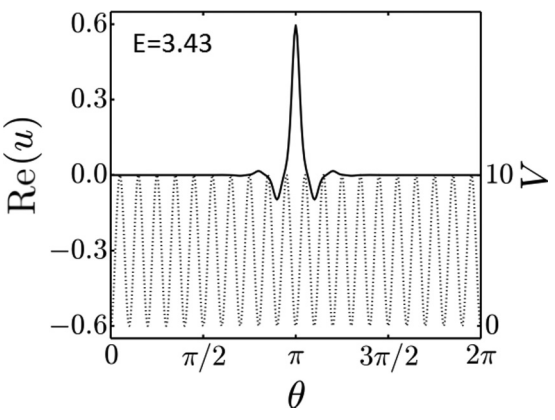

FIG. 2. Stationary lattice soliton formed from applying dissipation to an initial Gaussian wave packet (4) with $\gamma = 2$. The shape of the lattice soliton is very similar to those presented in [38]. The dotted line is the lattice V (see the scale on the right), with $V_0 = 10$.

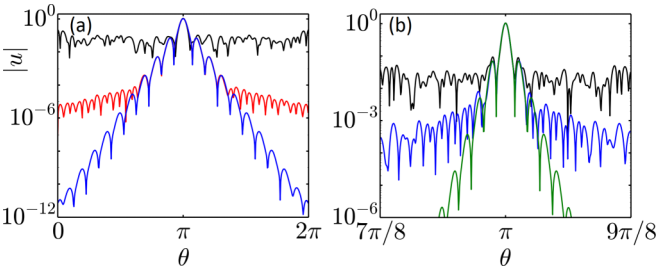

FIG. 3. Intensity distribution of stationary lattice solitons obtained from initial Gaussian wave packets with localized dissipation in a lattice of (a) 20 potential wells and (b) 160 potential wells. In (a), the curves correspond to $t = 0$ (black upper line), $t = 20\,000$ (red middle line), and $t = 100\,000$ (blue lower line), with time $t = 0$ corresponding to the moment dissipation is turned on. In (b), we also show $t = 0$ (black upper line) and$t = 100\,000$ (blue lower line), along with the intensity distribution after increasing the number of potential wells where the dissipation acts on from ∼4 to ∼150 at $t = 100\,000$ and then running the simulation for another 100 000 time units (green lower line).

noisy background, leading to exponential tails associated with lattice solitons. In the larger lattice, this effect is less obvious due to the distance from the lattice soliton to the place where the dissipation is applied [Fig. 3(b)]. Making the dissipation broader so that it acts on most of the potential wells in the lattice (in this case ∼150 out of 160) can help to reveal the tails faster [see green lower line in Fig. 3(b)].

We find that the final shape and frequency of the lattice soliton is affected by changing the initial width of the Gaussian γ: the wider the Gaussian is, the more atoms are lost due to dissipation and the lower the final peak amplitude of the lattice soliton is. The frequency of the oscillations of the real and imaginary parts of the solitons, along with the gradient of the exponential tails of the soliton, is larger if the number of atoms (i.e., the peak amplitude) is larger. This can be seen in Table I, where the peak intensity, gradient, and frequency of the final lattice soliton are displayed versus the Gaussian width.

Localized dissipations allow one to generate a broad variety of lattice solitons from Eq. (2). For example, for $\gamma = 1.3$ and $\gamma = 1.8$, the result is that of asymmetric lattice solitons with two high peaks next to each other (see Fig. 4). The oscillation of this asymmetric solution is quasiperiodic. The values of peak intensity, frequency, and gradient of the tails of the quasiperiodic solutions (QSs) in Table I are those

TABLE I. Values of parameters used in the simulations.

γ	Peak intensity	Gradient of tails	Frequency	Nature of solution
0.5	1.258	0.420	4.05	SLS
0.7	1.167	0.410	3.97	SLS
0.9	1.012	0.398	3.89	SLS
1.0	0.923	0.392	3.83	SLS
1.2	0.765	0.367	3.72	SLS
1.3	0.651	0.355	3.62	QS
1.6	0.539	0.332	3.55	SLS
1.8	0.377	0.289	3.46	QS
2.0	0.362	0.287	3.43	SLS

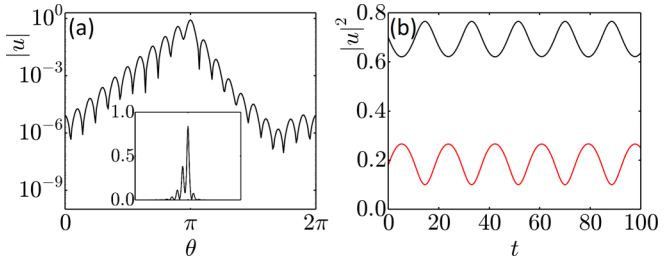

FIG. 4. (a) Quasiperiodic solution generated by applying dissipation to an initial Gaussian with width $\gamma = 1.3$. (b) Variation in time of intensity of peak of larger amplitude (black upper line) and smaller amplitude (red lower line).

associated with the highest peak in each case. Note that there are quasiperiodic discrete breather counterparts in the DNLSE (see [42]).

Another type of solution, shown in Fig. 5, is symmetric with two main peaks (as in [40]). The two peaks are in phase with each other and oscillate at the same frequency, as opposed to the previous quasiperiodic example in Fig. 4. This lattice soliton has been found by using localized dissipations and by shifting the initial wave packet by $L/2$ (half a potential well). The same effect can be obtained with a potential of $V = V_0 \cos^2(M\theta/2)$ rather than $V = V_0 \sin^2(M\theta/2)$, so that the initial Gaussian wave packet is centered between two potential wells. The nonlinearity is set to the value of $\beta = 10$, corresponding to a higher number of initial atoms or a larger scattering length. With $\beta = 1$, the double peak relaxes to the single-peak solution quickly.

For completeness we show that localized structures can also be obtained via localized dissipations by starting from a homogeneous distribution of atoms across the optical lattice with random phases in analogy with what has been done in the DNLSE [7,12]. In the example here, we first run a transient without dissipation for 1000 time steps. After this, dissipation is turned on, as shown in Fig. 6. There is a first localization to two peaks [see Fig. 7(a)]. The amplitudes of the peaks fluctuate and, eventually, at long time scales (around $t = 35\,000$), the peaks move closer to each other, so that only one potential well separates them [see Fig. 7(b)]. To observe this behavior the nonlinearity has been increased to $\beta = 50$.

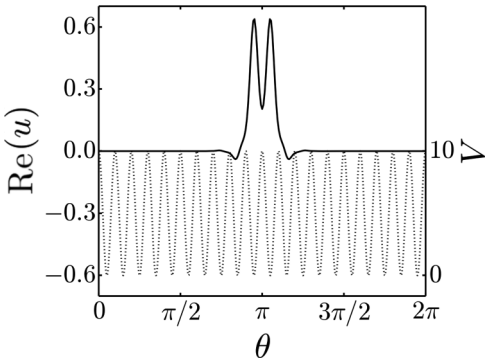

FIG. 5. A higher-order stationary soliton solution with two peaks formed from applying dissipation to an initial Gaussian wave packet (4) centered between two potential wells.

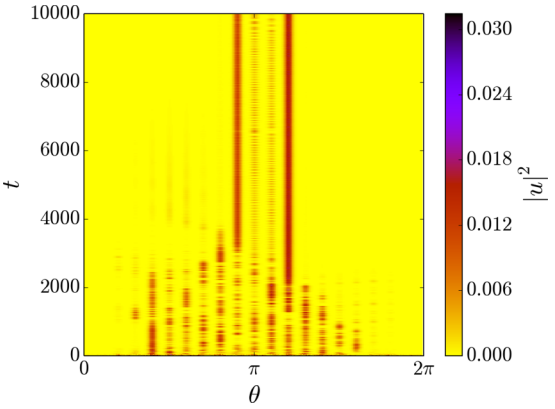

FIG. 6. Space-time evolution of atomic density $u(x,t)$ with $\beta = 50$ in the presence of localized dissipations. The initial condition is that of a "flat" equal amplitude wave function with random phases.

IV. TRAVELING LOCALIZED DISSIPATIONS

By using an initial Gaussian wave packet with an additional momentum, traveling breathers can be formed in the DNLSE [7,10,11]. In order to simulate this procedure in the continuous case and stabilize a TLS, we have used an initial distribution made of a "Gaussian of Gaussians" [see Fig. 8(a)]. In the DNLSE where each potential well corresponds to a single lattice point, our distribution reduces to a normal Gaussian shape [see dashed line in Fig. 8(a)]. With the addition of an initial momentum p [here set to $\cos(p) = -0.95$], a traveling peak is formed in the continuous model. We then apply dissipation in the angular position opposite this peak in a way similar to what is described in [7] for the DNLSE. Since the atomic density peak is traveling, the point at which dissipation is applied also moves.

In the example shown in Figs. 8 and 9, we consider $\beta = 1.0$, $V_0 = 10$, and $\cos(p) = -0.95$ with dissipations given by $\rho = 0.5$ over four lattice wells. At the beginning of the simulation, a certain number of atoms remain stationary after the traveling peak is formed. This can be seen in Fig. 8(b), with the high-amplitude stationary part of the wave function visible until $t \approx 100$, when these atoms are removed from the lattice by the moving dissipation beam. At long time scales, the peak shapes into a TLS that travels at a constant speed [shown in Fig. 9(a)]. It is important to note that without dissipation, the atoms that do not travel with the moving peak eventually spread across the lattice, giving rise to a large background noise. As

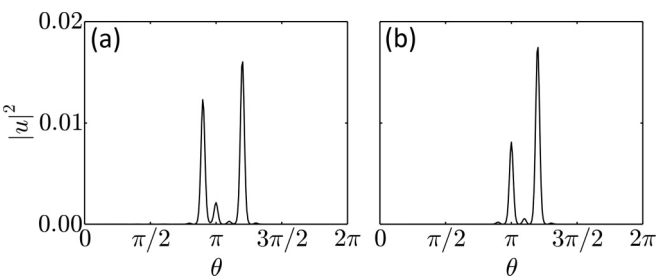

FIG. 7. Intensity distribution of localized solution obtained from applying dissipation to an initially flat wave function at (a) $t = 10\,000$ and (b) $t = 100\,000$.

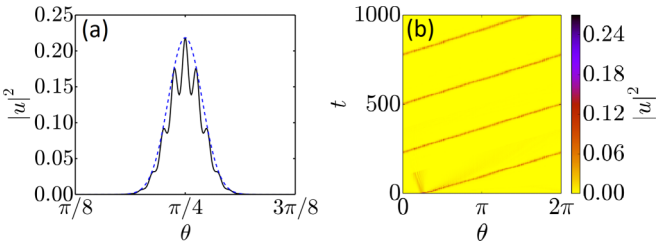

FIG. 8. (a) Initial condition for the formation of a TLS. Note that this distribution would be an ordinary Gaussian shape in the DNLSE (blue dashed line). (b) Space-time evolution of atomic density $u(x,t)$ of the TLS with $\Lambda = 1$ and dissipations $\rho = 0.5$.

the moving peak travels and interacts with the background, its amplitude reduces since it loses atoms to the background. By $t \approx 1600$, the height has decreased by half, and by $t \approx 3000$ the conservative traveling peak has disappeared. In contrast in the presence of the moving dissipation, the TLS survives on much longer time scales, maintaining the same height after $t \approx 40\,000$. The fact that dissipation helps instead of hinders the formation of a TLS is even more surprising since, different from the stationary lattice solitons, TLSs require the presence of a background in order to overcome the unavoidable Peierls–Nabarro barriers [7,43]. The presence of the localized dissipation is then twofold: on one side it removes enough stationary background noise to help with the localization of the TLS, and on the other it moves with the traveling background, thus keeping it at the level necessary for the motion and stability of the TLS.

It is important to note that the TLS of Fig. 9(a) formed via the localized dissipation is a higher-order TLS with two atomic density peaks per potential well [see Fig. 9(b)]. Due to its shape, this TLS has no counterpart in the DNLSE. We have determined an approximate form of the amplitude of the TLS displayed in Fig. 9 that can be used as the initial condition at time $t = 0$, given by

$$u(\theta) = -7.66A \exp\left[i\frac{pM(\theta-\pi)}{2\pi}\right] \times \sin[M(\theta-\pi)]\mathrm{sech}[AM(\theta-\pi)], \qquad (5)$$

where A is a parameter that depends on the width of the TLS. For $A = 1/(7.5\pi)$ and $p = -0.4$ we obtain a fit of the TLS

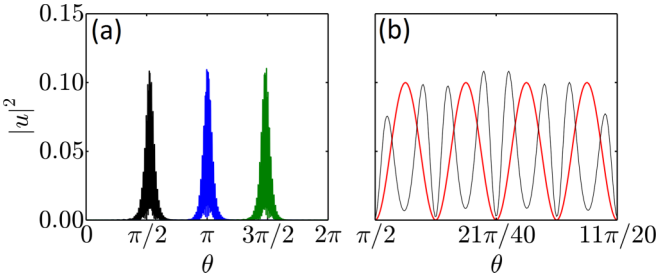

FIG. 9. (a) Intensity distribution of a TLS at $t = 10\,150$ (black left line), $t = 10\,220$ (blue middle line), and $t = 10\,290$ (green right line). (b) Close-up of intensity distribution at $t = 10\,150$ (black thin line) with the periodic potential (red thick line), showing the two peaks per potential well.

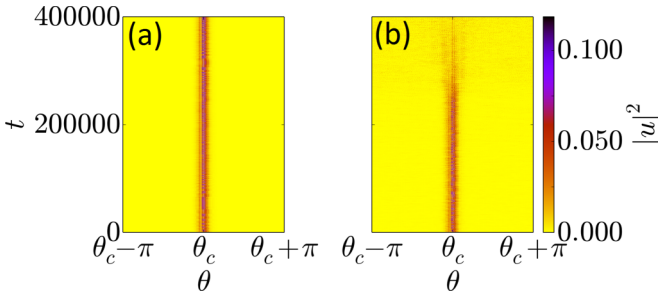

FIG. 10. Temporal evolution of the intensity distribution of the TLS initiated via (5) for the case (a) with localized dissipations ($\rho = -0.4$) and (b) without localized dissipations ($\rho = 0$). Note that TLS is traveling along the ring, but each distribution has been shifted to have the TLS maximum at the same angular location.

in Fig. 9 as accurate as a few percent. Having determined the approximate TLS shape in Eq. (5), one can use it as an initial condition for the formation of the double-peak TLS in the presence or absence of dissipation. With dissipation $\rho = 0.5$, we have verified that the TLS of Fig. 9 forms much faster when using the wave packet (5) as the initial condition instead of the Gaussian wave packet. Figure 10(a) shows that this TLS survives for extremely long time scales with an extremely small loss of atomic density or energy. The steady loss due to dissipation is so small that after 1 million time units, the atomic density only decreases by 0.21%. This is similar to what happens to the stationary lattice solitons in Sec. III when boundary losses approach irrelevance at the tails of the lattice soliton.

Without localized dissipation, a traveling peak starting from (5) survives for a long time [see Fig. 10(b)]. However, in the absence of dissipation, the background noise eventually grows and absorbs the peak, as shown in the last stages of Fig. 10(b). These features demonstrate that localized dissipation is necessary for both the formation and the stability of the double-peak TLS when starting from wave-packet distributions of atoms in the lattice with a given momentum.

We have also applied localized traveling dissipation to TLSs with one peak per potential well by using the analytical approximation of [44],

$$u(\theta) = 8.11A \exp\left[i\frac{pM(\theta-\pi)}{2\pi}\right] \times \cos\left[\frac{M(\theta-\pi)}{2}\right]\mathrm{sech}[AM(\theta-\pi)], \qquad (6)$$

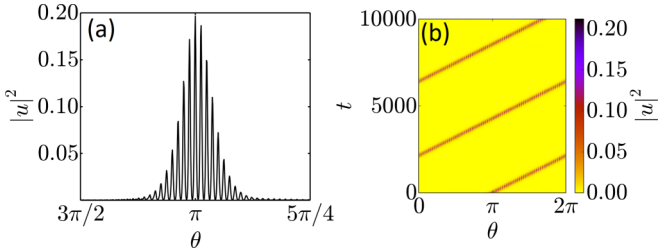

FIG. 11. TLS with one peak stabilized by localized dissipations.

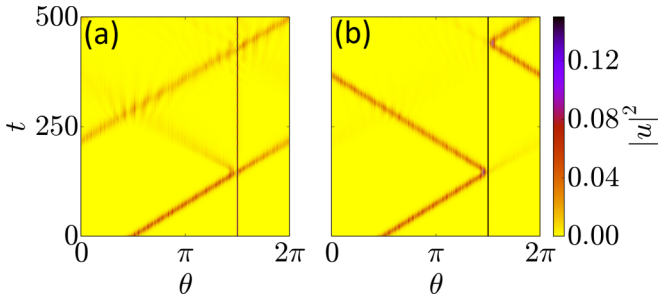

FIG. 12. A TLS colliding with a SLS of amplitude ≈0.45 (a) and ≈0.95 (b).

with A and p being the amplitude and the momentum of the TLS, respectively. In Figs. 11(a) and 11(b) we set $A = 0.3/(2\pi)$ and $p = -0.5$ and show the amplitude of the initial condition (6) and its temporal evolution in the ring, respectively. It is important to note that with or without dissipation, the initial condition (6) quickly develops a noisy background on which the TLS travels while remaining well approximated by (6) in the potential wells where atomic localization takes place. The dissipation clears up stationary noise but does not destroy the TLS with one peak per potential well. The atomic density is only slightly affected by the dissipation, which decreases by ∼0.12% after 1 million time units, even slower than the higher-order TLS.

V. COLLISION OF TRAVELING AND STATIONARY LATTICE SOLITONS

In this section we investigate the collision of the TLS with two peaks per potential well (previously stabilized by the localized dissipations) and a stationary lattice soliton (SLS) generated with the same method as discussed in Sec. III. The height of the stationary soliton is varied by changing the width of the initial Gaussian wave packet via a modification of the γ parameter.

In Fig. 12 the temporal evolution of the atomic density of both lattice solitons at successive collisions in the ring is displayed for zero dissipation. The TLS and the SLS are initially as far apart in the ring from each other as possible. The amount of atomic density that passes through the stationary lattice soliton at each collision is determined by its height. The higher the stationary lattice soliton is, the less atomic density passes through, as shown in the examples in Fig. 12. For example, when the amplitude of the SLS is low [see Fig. 12(a)], the majority of the atomic density in the TLS passes through the stationary one at the point of collision, with only a small amount being reflected. After each collision, the atomic density that has been reflected interferes with and scatters the atomic density of the TLS that has been transmitted by the SLS. This makes the TLS weaker and weaker as time goes on.

When the amplitude of the SLS is high [≈0.95 in Fig. 12(b)], the majority of the atoms in the TLS reflects off of the stationary one, while only a small number manage to tunnel through. The small amount of atomic density that tunnels through appears to have no major effect on the reflected TLS, which manages to survive longer than in the previous example.

VI. COLLISIONS OF TWO TRAVELING LATTICE SOLITONS

For completeness, we examine the collisions of two TLSs circling in the ring. In the first example, in Fig. 13, we use the TLS with two peaks per potential well, as described in Sec. IV, with $\beta = 1$ and $V_0 = 10$. We first position two identical TLSs at opposite sides of the ring (≈π rad apart), make them travel in opposite directions ($p = 0.5$ and $p = -0.5$, respectively), and then make them collide. Since dissipation would interfere with the process of collisions, we set $\rho = 0$ for both TLSs. As demonstrated in Fig. 10(b), the TLS with no dissipations survives for a long time, during which more than a hundred collisions can take place. We focus here on the first couple of collisions to establish the nature of the interaction of the TLSs at short distances and for interferometric properties. The collision of the two TLSs results in two seemingly identical TLSs at the output [see Fig. 13(a)]. We have verified that neither atomic density nor energy has changed in either of the output TLSs with respect to the input.

In order to find out if the TLSs have gone through one another or have reflected each other, we have split the wave function in two by substituting $u = u_1 + u_2$, where u_1 represents the atoms of one TLS and u_2 represents that atoms

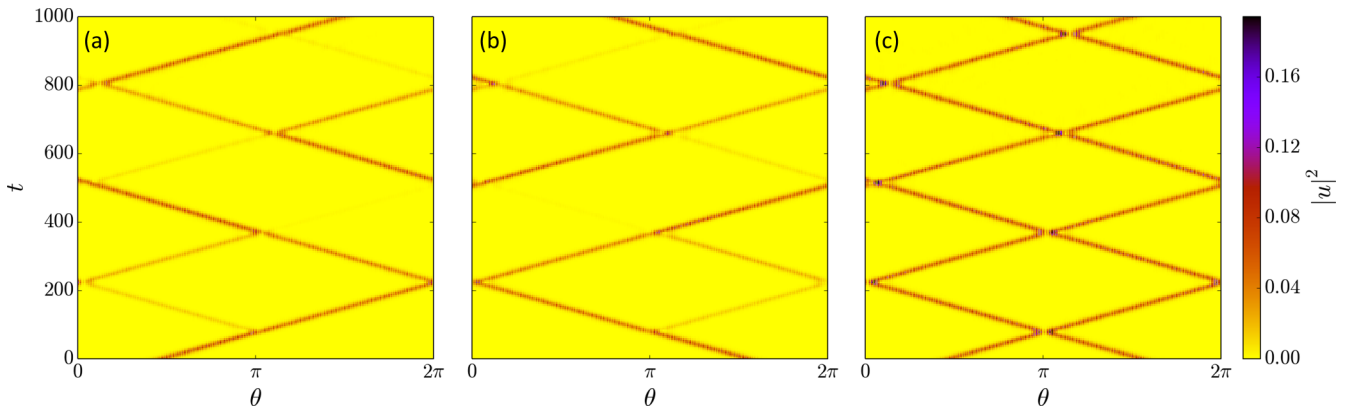

FIG. 13. Collision of two TLSs with two peaks per potential well. The total atomic density profile of the collisions is shown in (a), while the atomic density profile from each initial TLS is plotted in (b) and (c).

TABLE II. Percentage of atomic density reflected and transmitted in collisions between two higher-order TLSs.

V_0	Reflection	Transmission
7.0	11.8	88.4
7.5	12.6	87.4
8.0	13.7	86.3
8.5	15.1	85.0
9.0	16.8	83.2
9.5	18.6	81.5
10.0	20.4	79.6

in the other, into Eq. (2) to get

$$i\frac{\partial u_1(\theta,t)}{\partial t}=\left[-\frac{\pi^2}{2M^2}\frac{\partial^2}{\partial\theta^2}+V_0 sin^2\left(\frac{M\theta}{2}\right)+\beta|u_1+u_2|^2\right]u_1,$$

$$i\frac{\partial u_2(\theta,t)}{\partial t}=\left[-\frac{\pi^2}{2M^2}\frac{\partial^2}{\partial\theta^2}+V_0 sin^2\left(\frac{M\theta}{2}\right)+\beta|u_1+u_2|^2\right]u_2. \tag{7}$$

We find that, when the TLSs collide, some of the atomic density from each TLS passes through the other while the remaining part is reflected. When this happens, the reflected atomic density of one TLS merges with the transmitted part of the other one. This happens in such a way that the two TLSs that result from the collision have approximately the same shape as the original ones, despite containing a mixture of the atomic densities from both of them. We have verified that the results of the numerical simulations of Eqs. (7) reproduce exactly those of the simulations of Eq. (2) when considering $u = u_1 + u_2$. In this particular example, ∼79.6% of the atomic density of each TLS passes through the other one at each collision. The evolution of the atomic density distributions of each initial TLS is plotted in Figs. 13(b) and 13(c), showing how each TLS splits at each collision. The transmitted and reflected fractions of atomic density of the two TLSs in the collisions do not change when starting the collision process from a different initial location of the TLS. However, we have measured that these fractions change with the depth of the lattice potential, as reported in Table II.

Similar results of collisions occur with the TLSs with just one peak per potential well. In Fig. 14, we show collisions of these TLSs for $V_0 = 10$ and $\beta = 0.041$. Again, the TLSs "swap" atomic density at each collision, with the shape of the resulting TLSs largely unchanged. Here ∼77.0% of the atomic density in each TLS stays with the original one at each collision, while the remainder joins the other one. In Table III we show the dependence of the transmitted and reflected fractions of atomic density in the collisions of TLSs with a single peak per potential well when changing the depth of the optical lattice.

VII. CONCLUSIONS

We have analyzed the effect of local dissipation on BEC in a ring lattice. We found that the dissipation can both generate and stabilize stationary and traveling lattice solitons. A TLS with two intensity peaks per potential well was introduced that does not have a counterpart in the DNLSE. This can be generated via an initial Gaussian wave packet (as in the discrete model) with dissipation. This does not survive without losses in the long term. We then investigated the collisions of this TLS with different SLSs and found that the interaction and survival of the TLS depends on the amplitude of the SLS. We also analyzed the collisions of two TLSs in the ring. We found that some of the atoms in each TLS merge with the colliding one, while some are reflected in such a way that the shape of the resulting TLS's intensities stays the same. This collisional property depends on the potential depth of the lattice. The number of atoms that are transmitted (reflected) during the collision is smaller (larger) in deeper lattices and larger (smaller) in shallower lattices.

A possible application of the TLS in a ring lattice is interferometry. The TLS can collide with extra potential barriers added to the lattice. This has been proposed for attractive BECs without a lattice in [16–18]. With an optical lattice, there is the possibility for the interferometric features, such as Sagnac effects, to work with a repulsive BEC and with higher-order TLSs.

The SLS and TLS solutions obtained via localized dissipations are robust deterministic features to small fluctuations. It

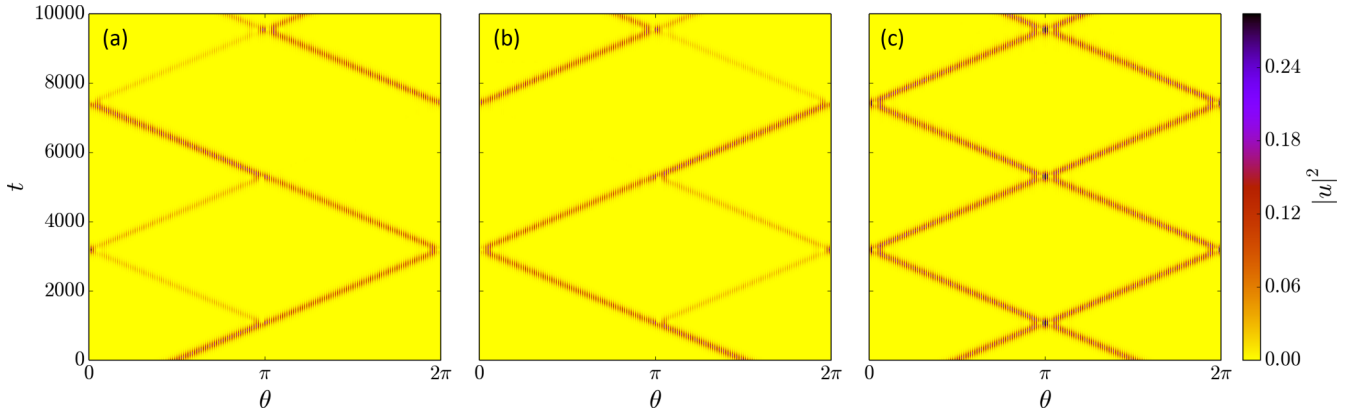

FIG. 14. Collision of two TLSs with a single peak per potential well. The total atomic density profile of the collisions is shown in (a), while the atomic density profile from each initial TLS is plotted in (b) and (c).

TABLE III. Percentage of atomic density reflected and transmitted in collisions between two TLSs.

V_0	Reflection	Transmission
9.0	14.7	85.3
9.5	18.3	81.7
10.0	23.0	77.0
10.5	29.5	70.5
11.0	38.2	61.8

should also be noted that although the model and equations of this paper have been used to describe the situation of BECs in a ring lattice, they can also be generalized to light propagating in cylindrical arrays of waveguides.

ACKNOWLEDGMENTS

R.C. acknowledges support from EPSRC DTA Grant No. EP/M506643/1.

[1] O. Morsch and M. Oberthaler, Rev. Mod. Phys. **78**, 179 (2006).
[2] I. Bloch, J. Dalibard, and W. Zwerger, Rev. Mod. Phys. **80**, 885 (2008).
[3] M. Greiner, O. Mandel, T. Esslinger, T. W. Hänsch, and I. Bloch, Nature (London) **415**, 39 (2002).
[4] M. L. Chiofalo and M. P. Tosi, J. Phys. B **34**, 4551 (2001).
[5] G. Roati, C. D'Errico, L. Fallani, M. Fattori, C. Fort, M. Zaccanti, G. Modugno, M. Modugno, and M. Inguscio, Nature (London) **453**, 895 (2008).
[6] D. A. Zezyulin, V. V. Konotop, G. Barontini, and H. Ott, Phys. Rev. Lett. **109**, 020405 (2012).
[7] R. Franzosi, R. Livi, G.-L. Oppo, and A. Politi, Nonlinearity **24**, R89 (2011).
[8] K. E. Strecker, G. B. Partridge, A. G. Truscott, and R. G. Hulet, Nature (London) **417**, 150 (2002); D. J. Frantzeskakis, J. Phys. A **43**, 213001 (2010).
[9] B. Eiermann, Th. Anker, M. Albiez, M. Taglieber, P. Treutlein, K.-P. Marzlin, and M. K. Oberthaler, Phys. Rev. Lett. **92**, 230401 (2004); Th. Anker, M. Albiez, R. Gati, S. Hunsmann, B. Eiermann, A. Trombettoni, and M. K. Oberthaler, *ibid.* **94**, 020403 (2005).
[10] H. Hennig, T. Neff, and R. Fleischmann, Phys. Rev. E **93**, 032219 (2016).
[11] A. Trombettoni and A. Smerzi, Phys. Rev. Lett. **86**, 2353 (2001).
[12] R. Livi, R. Franzosi, and G.-L. Oppo, Phys. Rev. Lett. **97**, 060401 (2006).
[13] G. S. Ng, H. Hennig, R. Fleischmann, T. Kottos, and T. Geisel, New J. Phys. **11**, 073045 (2009).
[14] R. Franzosi, R. Livi, and G.-L. Oppo, J. Phys. B **40**, 1195 (2007).
[15] G. D. McDonald, C. C. N. Kuhn, K. S. Hardman, S. Bennetts, P. J. Everitt, P. A. Altin, J. E. Debs, J. D. Close, and N. P. Robins, Phys. Rev. Lett. **113**, 013002 (2014).
[16] J. L. Helm, T. P. Billam, and S. A. Gardiner, Phys. Rev. A **85**, 053621 (2012).
[17] J. L. Helm, S. J. Rooney, C. Weiss, and S. A. Gardiner, Phys. Rev. A **89**, 033610 (2014).
[18] J. L. Helm, S. L. Cornish, and S. A. Gardiner, Phys. Rev. Lett. **114**, 134101 (2015).
[19] V. A. Brazhnyi, V. V. Konotop, V. M. Pérez-García, and H. Ott, Phys. Rev. Lett. **102**, 144101 (2009).
[20] W. H. Heathcote, E. Nugent, B. T. Sheard, and C. J. Foot, New J. Phys. **10**, 043012 (2008).
[21] L. Amico, A. Osterloh, and F. Cataliotti, Phys. Rev. Lett. **95**, 063201 (2005).
[22] S. Franke-Arnold, J. Leach, M. J. Padgett, V. E. Lembessis, D. Ellinas, A. J. Wright, J. M. Girkin, P. Ohberg, and A. S. Arnold, Opt. Express **15**, 8619 (2007).
[23] K. Henderson, C. Ryu, C. MacCormick, and M. G. Boshier, New J. Phys. **11**, 043030 (2009).
[24] S. Moulder, S. Beattie, R. P. Smith, N. Tammuz, and Z. Hadzibabic, Phys. Rev. A **86**, 013629 (2012).
[25] D. N. Christodoulides and R. I. Joseph, Phys. Rev. Lett. **62**, 1746 (1989); A. B. Aceves and S. Wabnitz, Phys. Lett. A **141**, 37 (1989); B. J. Eggleton, R. E. Slusher, C. M. de Sterke, P. A. Krug, and J. E. Sipe, Phys. Rev. Lett. **76**, 1627 (1996); H. S. Eisenberg, Y. Silberberg, R. Morandotti, A. R. Boyd, and J. S. Aitchison, *ibid.* **81**, 3383 (1998); D. Mandelik, R. Morandotti, J. S. Aitchison, and Y. Silberberg, *ibid.* **92**, 093904 (2004).
[26] Y. V. Kartashov, V. A. Vysloukh, and L. Torner, Prog. Opt. **52**, 63 (2009).
[27] Y. V. Kartashov, B. A. Malomed, V. A. Vysloukh, and L. Torner, Opt. Lett. **33**, 2949 (2008).
[28] B. A. Malomed, J. Opt. Soc. Am. B **31**, 2460 (2014).
[29] C. M. Bender and S. Boettcher, Phys. Rev. Lett. **80**, 5243 (1998).
[30] Y.-J. He and B. A. Malomed, in *Spontaneous Symmetry Breaking, Self-Trapping, and Josephson Oscillations*, edited by B. A. Maolomed (Springer, Heidelberg, 2013), p. 125; V. V. Konotop, J. Yang, and D. A. Zezyulin, Rev. Mod. Phys. **88**, 035002 (2016).
[31] R. J. C. Spreeuw, T. Pfau, U. Janicke, and M. Wilkens, Europhys. Lett. **32**, 469 (1995); N. P. Robins, P. A. Altin, J. E. Debs, and J. D. Close, Phys. Rep. **529**, 265 (2013).
[32] D. A. Zezyulin and V. V. Konotop, arXiv:1607.08439.
[33] M. Greiner, O. Mandel, T. Hänsch, and I. Bloch, Nature (London) **419**, 51 (2002).
[34] L. Pezzé and A. Smerzi, Phys. Rev. Lett. **102**, 100401 (2009).
[35] D. Witthaut, F. Trimborn, H. Hennig, G. Kordas, T. Geisel, and S. Wimberger, Phys. Rev. A **83**, 063608 (2011).
[36] H. Hennig and R. Fleischmann, Phys. Rev. A **87**, 033605 (2013).
[37] G. Kordas, S. Wimberger, and D. Witthaut, Phys. Rev. A **87**, 043618 (2013).
[38] N. K. Efremidis and D. N. Christodoulides, Phys. Rev. A **67**, 063608 (2003).
[39] I. E. Papacharalampous, P. G. Kevrekidis, B. A. Malomed, and D. J. Frantzeskakis, Phys. Rev. E **68**, 046604 (2003).

[40] P. J. Y. Louis, E. A. Ostrovskaya, C. M. Savage, and Y. S. Kivshar, Phys. Rev. A **67**, 013602 (2003).
[41] T. Gericke, P. Würtz, D. Reitz, T. Langen, and H. Ott, Nat. Phys. **4**, 949 (2008).
[42] M. Johansson and S. Aubry, Nonlinearity **10**, 1151 (1997).
[43] Y. S. Kivshar and D. K. Campbell, Phys. Rev. E **48**, 3077 (1993); J. Gòmez-Gardeñes, L. M. Floria, M. Peyrard, and A. R. Bishop, Chaos **14**, 1130 (2004).
[44] H. Sakaguchi and B. A. Malomed, J. Phys. B **37**, 1443 (2004).